

OrthoInsight: Rib Fracture Diagnosis and Report Generation Based on Multi-Modal Large Models

Jinzhi Wang, Jiangbo Zhang, Chenzhan Yu, Zhigang Xiu, Duwei Dai, Ziyu xu, Ningyong Wu, and Wenhong Zhao

Abstract—The growing volume of medical imaging data has increased the need for automated diagnostic tools, especially for musculoskeletal injuries like rib fractures, commonly detected via CT scans. Manual interpretation is time-consuming and error-prone. We propose OrthoInsight, a multi-modal deep learning framework for rib fracture diagnosis and report generation. It integrates a YOLOv9 model for fracture detection, a medical knowledge graph for retrieving clinical context, and a fine-tuned LLaVA language model for generating diagnostic reports. OrthoInsight combines visual features from CT images with expert textual data to deliver clinically useful outputs. Evaluated on 28,675 annotated CT images and expert reports, it achieves high performance across Diagnostic Accuracy, Content Completeness, Logical Coherence, and Clinical Guidance Value, with an average score of 4.28, outperforming models like GPT-4 and Claude-3. This study demonstrates the potential of multi-modal learning in transforming medical image analysis and providing effective support for radiologists.

Index Terms—OrthoInsight, Multi-modal large model, Rib fracture diagnosis, CT image analysis.

I. INTRODUCTION

THE advancement of medical imaging technologies has greatly improved the ability to detect and diagnose a wide range of medical conditions, particularly musculoskeletal injuries such as rib fractures [1]. Rib fractures are a common injury that can result from trauma or accidents and are often diagnosed through the use of computed tomography (CT) scans [2]. While traditional methods involving manual interpretation of CT images by radiologists have been widely employed, this process is inherently time-consuming, requires a high level of expertise, and is subject to human error [3]. As the volume of medical imaging data continues to grow, it has become increasingly difficult for radiologists to efficiently and accurately interpret every image. Recent studies demonstrate

J. Wang is with the Systems Engineering Institute, Xi'an Jiaotong University, No. 28, Xianning West Road, Beilin District, (e-mail: wangjz5515@stu.xjtu.edu.cn).

J. Zhang is with the School of Electronic Science and Engineering, Xi'an Jiaotong University, No. 28, Xianning West Road, Beilin District, Xi'an 710049, China (Corresponding author: Jiangbo Zhang, e-mail: 4522253009@stu.xjtu.edu.cn).

N. Wu, C. Yu, and Z. Xiu are with West China Longquan Hospital, Sichuan University, Chengdu, Sichuan, China.

D. Dai is with the Institute of Medical Artificial Intelligence, the Second Affiliated Hospital of Xi'an Jiaotong University, Xian, Shanxi, China.

Z. Xu is a Ph.D. candidate with the School of Human Settlements and Civil Engineering, Xi'an Jiaotong University, Xi'an, China. His main research areas include environmental science and engineering and applications of AI agent ecosystem projects (e-mail: Xzy365@stu.xjtu.edu.cn).

N. Wu and W. Zhao are with the Organizational Management Department, School of Management, Xi'an Jiaotong University, Xian, Shanxi, China. (e-mail: jdzhao@xjtu.edu.cn).

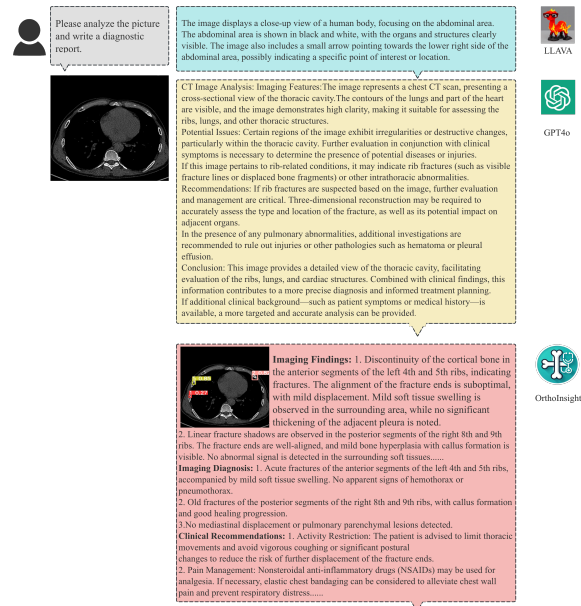


Fig. 1. Comparison of LLaVA, GPT-4V and OrthoInsight.

that AI-assisted workflows can significantly improve diagnostic sensitivity while maintaining high specificity [4]. This has created a significant need for automated systems that can assist clinicians in making accurate diagnoses more quickly and effectively.

In recent years, the development of artificial intelligence (AI) and deep learning techniques has shown considerable promise in revolutionizing medical image analysis. Among these, convolutional neural networks (CNNs [5]) and more advanced models, such as YOLO (You Only Look Once [6]), have become widely used for image detection tasks due to their ability to quickly identify objects within images with high accuracy. For example, improved YOLO variants achieve a mean average precision (mAP50) of 0.972 in rib fracture detection[7]. However, while these models excel at detecting visual features, the integration of contextual and domain-specific knowledge remains a critical challenge. In clinical practice, a diagnosis is often more than just a diagnosis of an issue: It requires understanding the underlying causes, possible treatment options, and the broader context of the patient's health. This gap in understanding has led to the emergence of multimodal learning approaches, which combine both image data and auxiliary text (such as clinical reports or medical knowledge) to generate more comprehensive output [8].

The application of multimodal learning to medical imaging holds significant potential in improving diagnostic accuracy and efficiency. By combining visual information from CT scans with textual data from expert reports and established medical knowledge, multi-modal models can generate detailed diagnostic insights that are not only more accurate but also more clinically actionable. For example, multimodal models can detect rib fractures, classify their type and severity, and generate automated diagnostic reports that include visual and textual descriptions, helping clinicians make informed decisions [9]. In this study, we propose a novel multimodal deep learning framework, OrthoInsight 1, specifically designed for the diagnosis of rib fractures from CT images. The framework integrates a YOLOv9-based model [10] to detect rib fractures on CT images, a medical knowledge graph to retrieve relevant clinical data, and a pre-trained language model (LLaVA) [11] to generate detailed and clinically useful diagnostic reports. This approach takes advantage of both visual feature extraction and domain-specific textual information, ensuring that the generated reports are accurate and useful for clinical practice. The primary contributions of this work are as follows:

- 1. We propose OrthoInsight, a robust multimodal framework that combines image features from CT scans with medical knowledge retrieved from expert reports and a knowledge graph to improve diagnostic accuracy.
- 2. We introduce a method for fine-tuning the LLaVA language model within OrthoInsight to generate detailed and clinically relevant diagnostic reports, ensuring both coherence and precision.
- 3. We evaluate the performance of OrthoInsight using a variety of standard metrics and demonstrate its ability to generate diagnostic reports that meet clinical standards and help in decision making.

II. RELATED WORK

A. Applications of Large Models in the Medical Field

The application of large-scale pre-trained models (e.g., GPT-4, Med-PaLM) in the medical field has made significant progress, particularly in medical text analysis and clinical decision support. In recent years, large language models (LLMs) based on natural language processing (NLP) have been widely used to handle tasks such as electronic health records (EHR), medical record summarization, and medical question-answering. LLMs, with their powerful text comprehension abilities, can automate the processing of large volumes of medical text and provide accurate clinical recommendations. For example, GPT-4 and Med-PaLM have made breakthroughs in medical question-answering tasks, especially in tests modeled after the United States Medical Licensing Examination (USMLE), achieving high scores (e.g. 86.4% precision for GPT-4 and 67.6% for Med-PaLM) and demonstrating their strong capabilities in understanding complex medical issues and clinical scenarios [12] [13]. Recent studies further validate that domain-specific LLMs such as Meditron-70B achieve performance comparable to general-purpose models while requiring fewer computational resources [14] [15].

In terms of question-answering capabilities, these models can also be applied to tasks such as medical text summarization and medical record information extraction. By training on large amounts of clinical text, LLMs can generate high-quality medical summaries, which hold great potential for reducing clinical documentation workload and improving efficiency. Research has shown that LLMs fine-tuned in the medical domain can generate summaries that are as accurate as, or even more accurate than, those written by human doctors (87% of clinicians rated LLM-generated summaries as equivalent or superior to human-written ones) [16] [15]. For instance, a hybrid model combining BART and rule-based post-editing improved radiology report summarization accuracy by 12% compared to standalone LLMs [17]. The applications of these models are not limited to extracting critical information to support clinical decision-making but also extend to providing personalized treatment plans for patients. As medical data continues to grow, systems that combine LLMs with medical knowledge graphs are gradually being deployed, assisting in diagnosis and decision-making by integrating multi-layered knowledge [18] [19]. A notable example is the use of dynamic knowledge graphs updated in real-time with EHR data, which enhanced treatment recommendation relevance by 23% in oncology cases [20]. Ethical and regulatory challenges remain critical. Studies highlight that over 30% of LLM-generated recommendations may contain biases related to patient demographics, emphasizing the need for rigorous fairness audits [21].

B. Applications of Multimodal Large Models in Medical Image Analysis

The use of multimodal large models (e.g., LLaVA, Med-Alpaca) in medical image analysis has become an important area of current research [8] [22]. Traditional medical image analysis methods typically rely solely on image data, often overlooking critical information from text data, such as radiology reports and clinical notes [23]. However, medical images often provide only local visual information, whereas a patient's medical history, clinical symptoms, and the physician's initial diagnosis are often key to making an accurate diagnosis [8]. To address this, multimodal large models combine image data and text data, significantly improving the accuracy of automated diagnosis [24].

In the field of medical imaging, multimodal large models primarily process both image and related text data through joint training of visual and language models. For example, the LLaVA-Med model enhances the understanding of medical images by leveraging multimodal learning. Trained on biomedical image and description datasets, the model can simultaneously process medical images and clinical text, generating more accurate image analysis reports. Moreover, approaches based on visual-language models (VLMs), such as GPT-4V, can recognize visual features in medical images and use language processing techniques to interpret and analyze these features [25] [23].

Furthermore, combining knowledge graphs with large models further enhances the quality of image analysis [26].

Integrating systems with medical ontologies like LS and SNOMED CT enables better understanding of the clinical context behind medical images and provides doctors with more precise and interpretable diagnostic suggestions [27]. This integration makes large models not only perform well in image classification and segmentation tasks but also excel in disease diagnosis, treatment recommendations, and follow-up care [28].

III. TASK SETUP

This task generates a detailed diagnostic analysis report from CT rib images. The input consists of a CT rib image and a prompt to guide the model in generating the report. The output is a diagnostic report containing image findings, image diagnosis, and clinical recommendations. The mathematical formulation is as follows:

$$R = \text{Gen}(\text{Fuse}(\text{ImgFeat}(I), \text{TxtEnc}(P))) = (T, C, S) \quad (1)$$

In this equation, R represents the generated report, $\text{ImgFeat}(I)$ refers to the image feature extractor applied to the CT rib image I , and $\text{TxtEnc}(P)$ refers to the text encoder used to process the prompt P . The function Fuse combines the image features and text encoding. GenReport is the report generation function. The generated report R consists of three main components: T represents image findings, C represents image diagnosis, and S provides clinical recommendations.

A. Evaluation metrics

In the general domain, evaluation metrics typically focus on text similarity, which may not fully address the specific requirements of the medical field, such as the precise use of medical terminology, the clinical practicality of treatment recommendations, and the logical rigor of the report. Therefore, to ensure that diagnostic reports effectively support clinical practice, specialized evaluation metrics must be established. Based on the professional opinions of orthopedic experts, practical application needs, and relevant evaluation standards from healthcare [29] [30], education [31], and software engineering [32] fields, we have identified four core characteristics that diagnostic reports should possess to ensure their reliability and clinical applicability in medical settings:

- 1) **Diagnostic Accuracy** evaluates the correctness of the diagnostic conclusions in the report, particularly the ability to accurately identify the type, location, and severity of rib fractures. A high-quality report should provide a detailed description of the fracture type, location, and healing status, such as: “Non-displaced fracture of the left 5th rib anterior segment, with bone callus growth, no pneumothorax or hemothorax.” A low-quality report may omit key information or make incorrect diagnoses, such as: “Left rib fracture,” without providing specific location, type, or severity, which can affect treatment decisions. Accurate diagnostic conclusions are critical for clinical decision-making, making diagnostic accuracy a core metric for report quality.

- 2) **Content Completeness** evaluates whether the report covers all necessary medical information, including image findings, diagnostic conclusions, relevant medical knowledge, and treatment recommendations. A high-quality report should comprehensively describe imaging features, diagnostic results, and treatment plans, for example: “CT shows a fracture of the left 5th rib anterior segment, with bone callus growth, recommended re-examination in 4 weeks.” A low-quality report may omit crucial information, such as merely stating “left rib fracture,” without detailing fracture type, location, or severity, which affects clinical judgment and treatment decisions. Therefore, the completeness of report content is essential for ensuring accurate diagnosis and treatment.
- 3) **Logical Coherence and Consistency** evaluates whether the report has a rational structure, clear hierarchical organization, and coherent expression. A high-quality report should follow a clear logical sequence, such as imaging findings \rightarrow diagnostic conclusions \rightarrow clinical recommendations, ensuring smooth content flow that is easy to understand. For example: “CT shows a fracture of the left 5th rib anterior segment, with bone callus growth, recommended re-examination in 4 weeks.” A low-quality report may suffer from confusion or lack of structure, making it difficult for readers to quickly extract key information, such as: “Fracture, rest recommended. CT shows left 5th rib fracture.” Logical coherence and consistency ensure that the report is easy for clinicians to interpret, enabling accurate clinical decision-making.
- 4) **Clinical Guidance Value** evaluates whether the report provides clear and actionable treatment recommendations to help formulate appropriate treatment plans and follow-up schedules. A high-quality report should provide specific treatment suggestions, such as: “It is recommended that the patient limit thoracic activity, use NSAIDs for pain relief, and re-evaluate the fracture healing status with CT in 4 weeks.” A low-quality report may lack detailed treatment plans or provide vague suggestions, such as: “Patient has a fracture, recommended rest, regular follow-up.” This metric focuses on whether the report has practical clinical value, helping physicians make informed clinical decisions.

Based on these metrics, we have established a scoring system with a range from 1 to 5 (as detailed in Table I), representing evaluation levels from low to high, to ensure the independence, objectivity, and scientific rigor of the evaluation process. These metrics ensure that rib fracture diagnostic reports are not only accurate but also clinically practical, helping to improve diagnostic accuracy and providing reliable references for clinical treatment.

IV. DATASET CONSTRUCTION

A. Data source

The data used in this study are primarily sourced from three main aspects:

- 1) **CT Image Dataset:** The dataset consists of publicly available rib fracture CT images provided by multiple

TABLE I
DETAILED SCORING CRITERIA FOR METRICS

Metrics	Scoring details
Diagnostic Accuracy (DA)	<p>5 points: Accurately identifies the type, location, and severity of the rib fracture. The diagnosis is correct and provides sufficient support for clinical decision-making.</p> <p>4 points: The diagnosis is accurate, recognizing the type, location, and severity of the fracture, but the description may be slightly brief or lack some details.</p> <p>3 points: Able to identify the type or location of the fracture but lacks a description of the severity, or the information is unclear.</p> <p>2 points: The diagnosis is vague or incomplete, failing to accurately identify the fracture type, location, or severity, and may lack crucial information.</p> <p>1 point: The diagnosis is incorrect or missing, failing to identify the fracture type, location, or severity, which impacts clinical treatment decisions.</p>
Content Completeness (CC)	<p>5 points: The report includes all necessary orthopedic information, including imaging findings, diagnosis, treatment recommendations, and follow-up plans. The content is comprehensive and detailed.</p> <p>4 points: The report includes most of the key information, with a few minor details missing, but still provides effective support for clinical decision-making.</p> <p>3 points: The report lacks some essential information, affecting the diagnosis and treatment decisions, though some conclusions can still be inferred from other parts.</p> <p>2 points: The report is incomplete, missing key details regarding the diagnosis or treatment plan, which affects clinical judgment.</p> <p>1 point: The report severely lacks critical information and cannot effectively support clinical decisions.</p>
Logical Coherence and Consistency (LCC)	<p>5 points: The report has a clear structure with well-organized information, following a logical sequence such as imaging findings → diagnosis → clinical recommendations, making it easy to understand.</p> <p>4 points: The report is generally well-structured with relatively coherent information. Minor structural issues may exist, but it remains understandable overall.</p> <p>3 points: The report's structure is somewhat disorganized, and the information is not clearly arranged, which affects understanding and the effective extraction of key information.</p> <p>2 points: The report lacks a clear structure, and the sequence of information is chaotic, making it difficult to understand or extract key points.</p> <p>1 point: The report is completely disorganized, lacking basic logical structure, difficult to understand, and cannot provide effective support for clinical decision-making.</p>
Clinical Guidance Value (CGV)	<p>5 points: Provides specific and effective treatment recommendations that clearly guide the clinician's treatment plan and follow-up strategy, offering high clinical value.</p> <p>4 points: Provides some treatment recommendations, though they may be somewhat general or lacking in detail, still offering useful support for clinical decisions.</p> <p>3 points: Treatment recommendations are not sufficiently clear or lack key details, potentially impacting the treatment plan, but still provide some guidance.</p> <p>2 points: Treatment recommendations are overly simplistic or unclear, lacking specificity, and may impact clinical decision-making.</p> <p>1 point: The report severely lacks critical information and cannot effectively support clinical decisions.</p>

medical institutions, comprising approximately 28,675 high-definition CT images. All images underwent standardized preprocessing, including resizing to 512×512 pixels and contrast enhancement using windowing techniques. The images are annotated with YOLO-format labels, where the annotations are provided in relative coordinates. These annotations cover five types of rib fractures: displaced rib fractures, non-displaced rib fractures, buckle fractures, segmental rib fractures, and uncertain-type rib fractures. The dataset ensures accurate localization and classification of the fracture regions in the detection task.

- 2) **Expert Diagnosis Report Dataset:** This study collected preliminary diagnosis reports written by five radiologists from Huaxi Hospital Longquan Hospital based on the CT images. These reports were formatted uniformly and underwent text cleaning, establishing a one-to-one correspondence with the corresponding CT images. The reports reflect the experts' initial judgments and clinical experience regarding the fracture features in the images, providing professional references for subsequent report generation.

- 3) **Rib Orthopedic Knowledge Base:** The rib orthopedic knowledge base was constructed by orthopedic experts from Huaxi Hospital Longquan Hospital, based on authoritative sources such as "Surgery" and the "Rib Fracture Diagnosis and Treatment Guidelines." This knowledge base systematically organizes multidimensional medical information on fracture classification, etiology, injury mechanisms, clinical manifestations, treatment plans, and management of complications. The knowledge graph is stored in a structured format, providing authoritative support for knowledge retrieval in the multimodal diagnostic report generation process.

B. Data Augmentation

Despite the availability of YOLO-based fracture labels and preliminary diagnostic reports, these data alone are insufficient to support the training of a multimodal large model for rib fracture diagnosis. To generate more comprehensive and detailed diagnostic reports, we have adopted successful practices from healthcare and education fields, utilizing GPT technology to enhance the diagnostic reports. The specific method is outlined as follows:

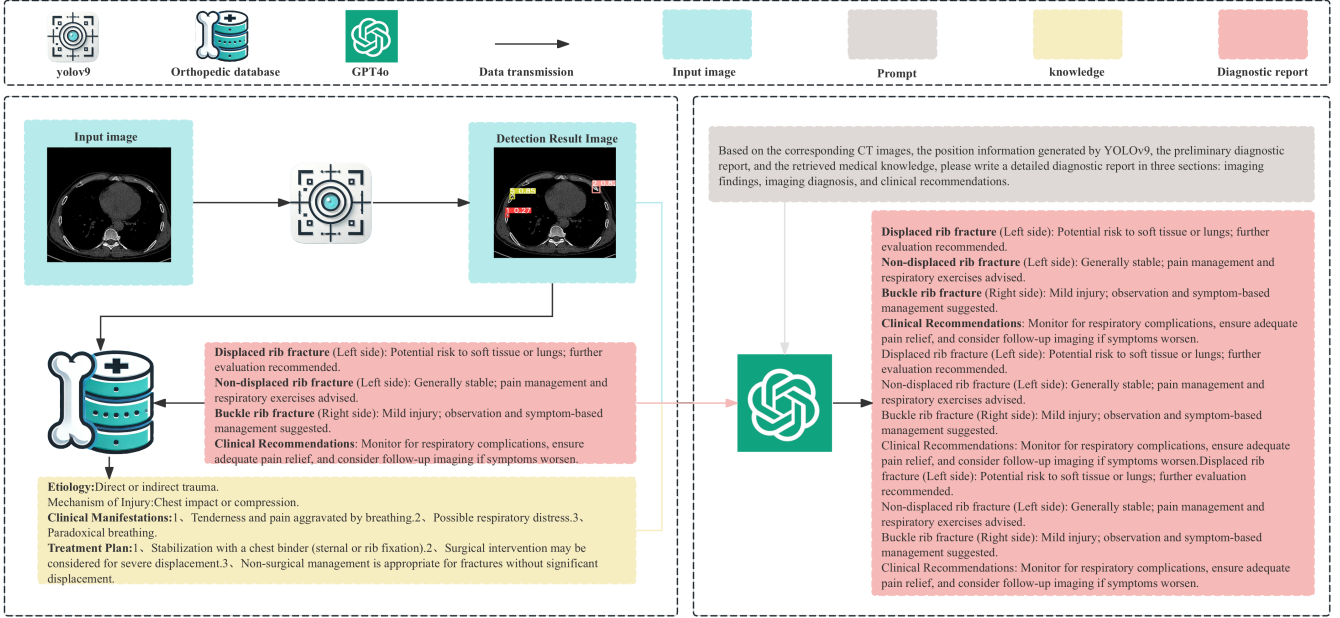


Fig. 2. Data construction diagram

First, the CT images are input into the YOLOv9 model to extract fracture location information and type labels. These results, combined with the existing preliminary diagnostic reports, are used to perform relevant knowledge retrieval from the rib orthopedic knowledge base (the specific retrieval method is described in Section 5.2). Next, we integrate the CT images, the location information generated by YOLOv9, the preliminary diagnostic reports, and the retrieved medical knowledge into a complete prompt. This prompt is then input into the GPT-4O model to generate a more detailed and clinically relevant diagnostic report. This process provides more comprehensive training samples for subsequent model training (see Figure 2).

C. Dataset Evaluation

Based on the study by Wang et al., this research adopts a large language model (LLM) as an automatic scoring tool to reduce reliance on manual evaluation. Specifically, we randomly selected 1,000 samples from the dataset and used GPT-4O to evaluate them according to predefined scoring criteria. Additionally, five orthopedic experts with extensive clinical experience independently evaluated 200 samples and assessed various metrics. Given the wide range of scoring criteria and the potential variability among evaluators, we used Cohen’s Kappa coefficient [33] to measure the consistency of scores. The Kappa coefficient ranges from -1 (completely disagree) to 1 (completely agree), with 0 indicating agreement by chance. The experimental results show that the Kappa value between GPT-4O-generated scores and expert scores was 0.74, while the Kappa value between different experts was 0.82. This indicates a high level of consistency between evaluators and between the model and expert evaluations, validating the reliability of the evaluation method (detailed scores are shown

in Table II). Furthermore, the average expert score was 4.23, and the average GPT-4O score was 4.31, further demonstrating that the enhanced diagnostic reports are of high quality and can serve as effective training samples for the model.

Model	DA	CC	LCC	CGV
GPT4 scorer	3.67	3.92	4.01	3.94
Expert rating	3.72	3.94	3.89	4.04

TABLE II
DATASET SCORING

V. EXPERIMENTAL METHODOLOGY

A. Rib Fracture Detection Model Training

To accurately detect the location and type of rib fractures in CT images, this study employs the YOLOv9 model for object detection. We used an annotated dataset that includes various types of rib fractures, such as displaced and non-displaced fractures. Each CT image in the dataset is precisely annotated, providing information on the fracture type and location. To optimize the model’s detection performance, all input CT images are first preprocessed, which includes resizing the images to 512x512 pixels and applying contrast enhancement techniques to highlight the fracture regions. This preprocessing step helps YOLOv9 effectively recognize and localize the fractures.

During the training process, YOLOv9 extracts features from the CT images and learns to identify the specific location and type of fractures. To ensure detection accuracy, we used cross-entropy loss as the loss function and applied the Adam optimizer to adjust the model’s parameters. The training process aims to improve the model’s fracture detection capabilities, enabling it to handle a variety of fracture types and locations.

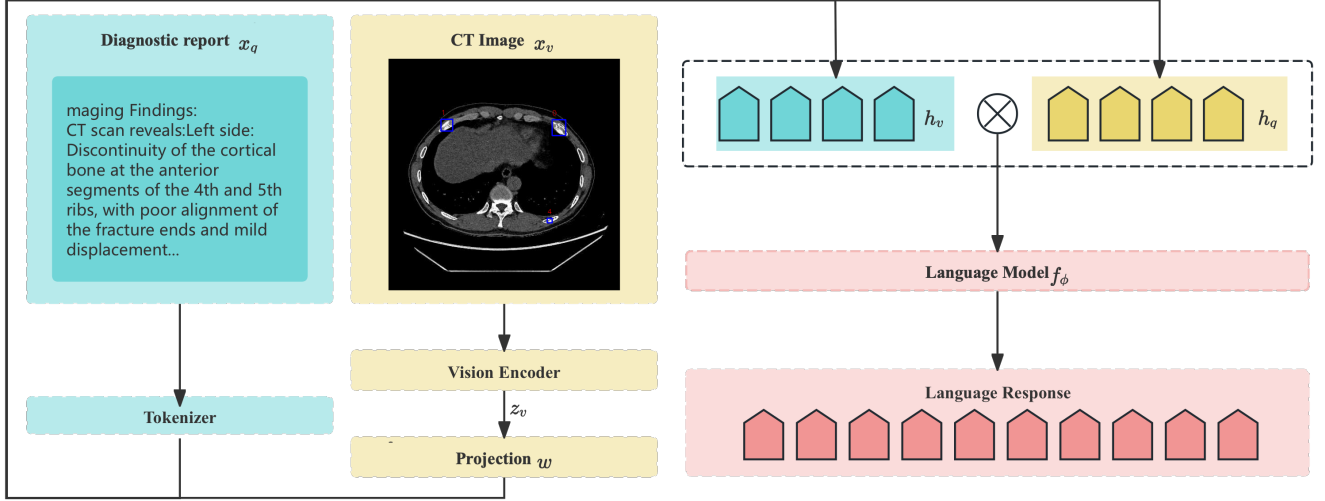


Fig. 3. Model architecture diagram

Through these training steps, the YOLOv9 model is able to efficiently extract fracture location information and type labels from new CT images. Once trained, the model provides accurate fracture localization and classification, which serves as key information for the subsequent diagnostic report generation.

B. Knowledge Retrieval Methodology

This section describes a knowledge retrieval and integration method based on the orthopedic knowledge base to enhance the diagnostic capability for rib fractures. The method consists of the following key steps: fracture type extraction and sub-knowledge base selection, query text construction, query vector encoding, knowledge node embedding construction, and similarity-based knowledge retrieval.

Fracture Type Extraction and Sub-Knowledge Base Selection: Based on the YOLO detection results, let T represent the set of detected rib fracture types:

$$T = \{t_1, t_2, \dots, t_m\}$$

For example, if the detected fracture types include "displaced rib fractures" and "segmental rib fractures", then:

$$T = \{\text{displaced rib fractures, segmental rib fractures}\}$$

For each fracture type $t \in T$, we select the corresponding sub-knowledge base K_t , which contains orthopedic information related to the fracture type, such as classification, etiology, injury mechanism, clinical manifestations, treatment plans, and complication management.

Query Text Construction: Let x_E represent the preliminary diagnostic report text written by experts. Simultaneously, using the mapping function $\text{map}_t(\cdot)$, we extract fracture-related descriptive information $x_{D,t}$ from the detection results. The final query text $x_{Q,t}$ is constructed as:

$$x_{Q,t} = x_E \oplus x_{D,t}$$

where \oplus represents the text concatenation operation.

Query Vector Encoding: A pre-trained orthopedic text encoder $f(\cdot)$ (such as a BERT encoder fine-tuned for the orthopedic domain) is used to map the query text to the vector space, resulting in the query vector:

$$q_t = f(x_{Q,t}) \in \mathbb{R}^d$$

where d is the dimension of the vector embedding.

Knowledge Node Embedding Construction: In the sub-knowledge base K_t , each orthopedic knowledge node i contains structured orthopedic information related to the fracture type. Its text representation x_i is constructed as:

$$\begin{aligned} x_i = & x_{\text{classification},i} \oplus x_{\text{etiology},i} \\ & \oplus x_{\text{injury mechanism},i} \oplus x_{\text{clinical manifestations},i} \\ & \oplus x_{\text{treatment plan},i} \oplus x_{\text{complication management},i} \end{aligned}$$

Then, using the same text encoder $f(\cdot)$, the text representation is converted into an embedding vector:

$$v_i(t) = f(x_i) \in \mathbb{R}^d$$

Similarity-Based Knowledge Retrieval: For each detected fracture type t , the query vector q_t and the knowledge node embedding vector $v_i(t)$ are compared using cosine similarity:

$$\text{sim}(q_t, v_i(t)) = \frac{q_t \cdot v_i(t)}{\|q_t\| \|v_i(t)\|}$$

Then, in the sub-knowledge base K_t , the top k knowledge nodes with the highest similarity are selected to form the candidate set:

$$C_t = \{i \mid \text{sim}(q_t, v_i(t)) \text{ ranks in the top } k\}$$

where C_t represents the candidate knowledge node set for fracture type t .

Final Knowledge Retrieval Output: For all detected fracture types $t \in T$, this method retrieves the corresponding

candidate knowledge sets C_t , which provide important information to support the multimodal diagnostic report generation.

By integrating fracture detection results, expert-written reports, and orthopedic knowledge base, this method not only improves the accuracy of diagnostic reports but also ensures that the model output aligns with authoritative knowledge in the orthopedic field, enhancing the interpretability and clinical reliability of the diagnostic results.

C. Model Architecture and Training Stages

1) *Model Architecture:* We adopted LLaVA, a multimodal dialogue model in the general domain, as the initial general language model (LM) for this study. The model architecture is shown in Figure 3 and architecture consists of three main components: a pre-trained vision encoder (ViT), a lightweight projection module (Proj), and a pre-trained large language model (LLM). Specifically, the CT image X_v and the diagnostic report text x_q are processed as follows: The CT image is first passed through the vision encoder to obtain visual feature representations Z_v , which are then mapped into visual embeddings h_v using the projection matrix W . Meanwhile, the diagnostic report x_q is tokenized by the Tokenizer, resulting in the text feature representation h_q . Next, the visual embeddings h_v and text embeddings h_q interact, typically through a dot product operation (\odot), to generate a joint representation. This joint representation is then passed through the pre-trained language model f_ϕ to generate the final diagnostic report y .

This process can be expressed by the following formula:

$$\text{Language Response} = f_\phi(W \cdot \text{Encoder}(X_v) \odot \text{Tokenizer}(x_q))$$

2) *Model Training Phases:* The training process is divided into two stages:

- 1) **Stage 1: Orthopedic Concept Feature Alignment:** In this stage, we freeze the weights of the vision encoder and the language model and only update the projection matrix. The goal is to align the visual embeddings with the word embeddings in the pre-trained large language model (LLM). This allows us to align a large number of orthopedic-related visual concepts with the text embeddings in the pre-trained language model, thereby enhancing the model’s understanding of the orthopedic domain.
- 2) **Stage 2: Instruction Fine-Tuning:** In the second stage, we freeze the vision encoder weights and continue to update the projection layer and the pre-trained weights of the LLM. The model is fine-tuned using augmented CT image-diagnostic report instruction-following data. This stage employs an end-to-end training approach to further optimize the model’s performance.

D. Inference Phase for Rib Fracture Diagnosis

After the training phase, the system enters the inference stage, where the trained model is applied to real CT images to generate diagnostic reports for rib fractures. The specific flowchart is shown in Figure 4. The inference process consists of the following key steps:

- 1) The CT images to be analyzed are input into the YOLOv9 model for fracture detection. The YOLOv9 model outputs fracture location information (i.e., the bounding boxes of the fractures) and fracture types (such as displaced fractures, non-displaced fractures, etc.).
- 2) The fracture location information and fracture type obtained from YOLOv9 are input into the orthopedic knowledge base for relevant knowledge retrieval. The orthopedic knowledge base contains related orthopedic information for different types of fractures, such as fracture causes, injury mechanisms, treatment plans, and complication management.
- 3) The CT image fracture location information, fracture type, and the orthopedic knowledge retrieved from the knowledge base are input into the trained LLaVA 1.5-7B model. The model combines image features, textual descriptions, and orthopedic knowledge to generate a detailed diagnostic report. The report includes a detailed description of the fracture, treatment recommendations, possible complications, and follow-up plans.

E. Inference Phase for Rib Fracture Diagnosis

After the training phase, the system enters the inference stage, where the trained model is applied to real CT images to generate diagnostic reports for rib fractures. The specific flowchart is shown in Figure 4. The inference process consists of the following key steps:

- 1) The CT images to be analyzed are input into the YOLOv9 model for fracture detection. The YOLOv9 model outputs fracture location information (i.e., the bounding boxes of the fractures) and fracture types (such as displaced fractures, non-displaced fractures, etc.).
- 2) The fracture location information and fracture type obtained from YOLOv9 are input into the orthopedic knowledge base for relevant knowledge retrieval. The orthopedic knowledge base contains related orthopedic information for different types of fractures, such as fracture causes, injury mechanisms, treatment plans, and complication management.
- 3) The CT image fracture location information, fracture type, and the orthopedic knowledge retrieved from the knowledge base are input into the trained LLaVA 1.5-7B model. The model combines image features, textual descriptions, and orthopedic knowledge to generate a detailed diagnostic report. The report includes a detailed description of the fracture, treatment recommendations, possible complications, and follow-up plans.

VI. EXPERIMENTAL SETUPS

A. Datasets

We evaluate all models on a proprietary multi-source heterogeneous rib-fracture dataset: it comprises 28 675 chest CT scans at 512×512 resolution, each annotated in YOLO format with five fracture subtypes—displaced, non-displaced, buckle, segmental, and indeterminate. All samples are divided 7:2:1 into training, test, and validation sets. To provide textual supervision, we also collect the original preliminary radiology

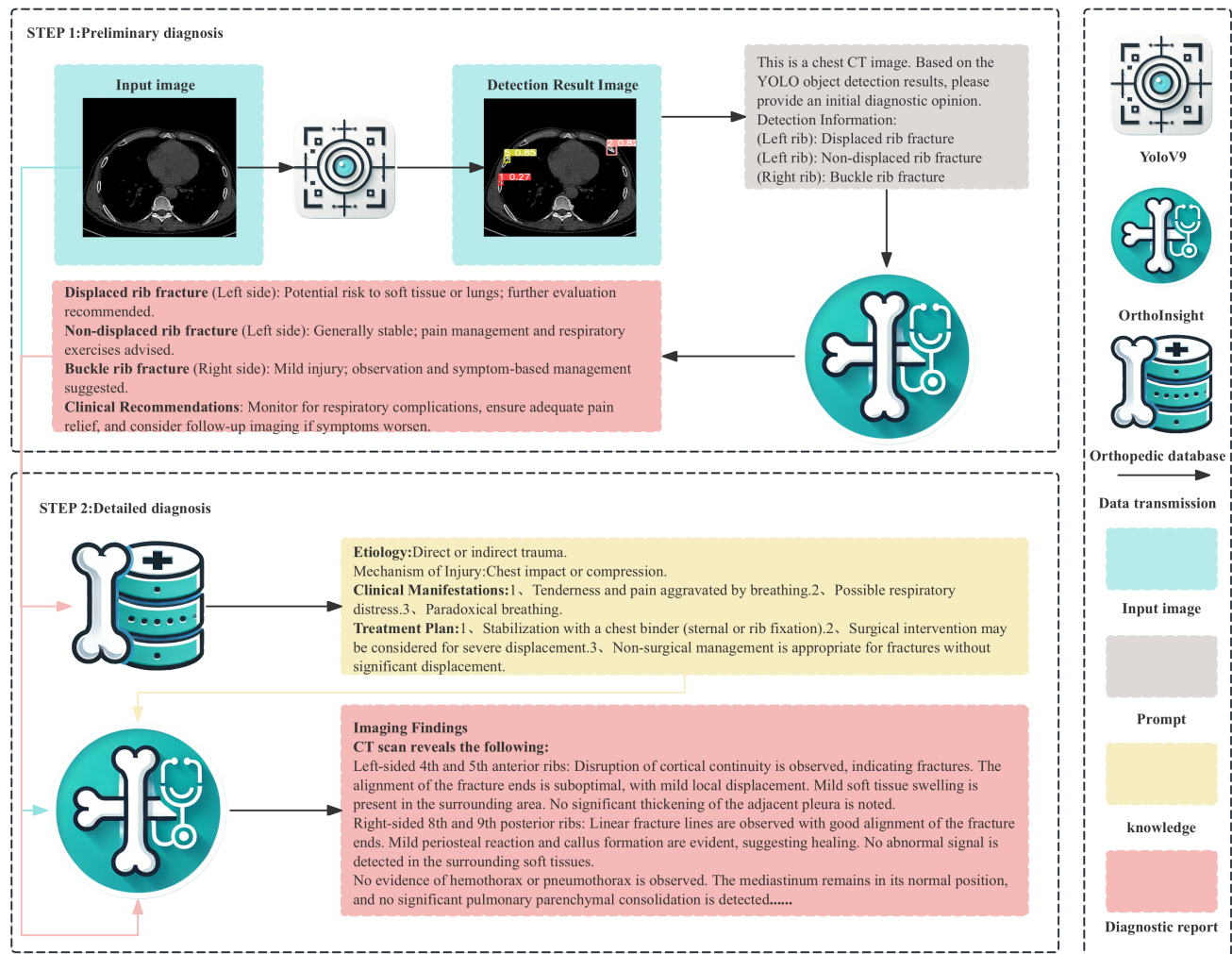


Fig. 4. Diagnostic flow chart

reports authored by five chief radiologists from tertiary hospitals. In addition, an orthopaedic knowledge graph containing six node types and about 42 k triples is curated from Surgery and the Guideline for Rib-Fracture Management to support medical facts. During preprocessing, YOLOv9 first localises and classifies fracture sites; its outputs, together with the expert reports and retrieved graph facts, are merged via a templated prompt and expanded into structured, fine-grained diagnostic reports, which serve as the training targets for the report-generation task.

B. Evaluation Metrics

a) Detection.: For the rib-fracture detection task, we follow the standard object-detection protocol and report four metrics: **Precision (P)**, **Recall (R)**, **mAP@0.5** (mean Average Precision at an IoU threshold of 0.5), and **mAP@0.5:0.95** (mAP averaged over IoU thresholds 0.50–0.95 in steps of 0.05). The metric mAP@0.5 measures overall detection accuracy when $\text{IoU} \geq 0.50$, whereas mAP@0.5:0.95 is more stringent and reflects the model’s sensitivity to localisation errors. All scores

are computed on the test split using the official COCO/YOLO evaluation script.

b) Report generation.: Quality of the generated diagnostic reports is assessed with a four-dimensional rubric recommended by orthopaedic specialists, comprising **Diagnostic Accuracy (DA)**—correctness of fracture type and anatomical location; **Content Completeness (CC)**—inclusion of image findings, diagnostic conclusion, and follow-up advice; **Logical Coherence & Consistency (LCC)**—structural clarity and narrative fluency; and **Clinical Guidance Value (CGV)**—practical utility of the recommended treatment plan. Each criterion is rated on a five-point Likert scale (1=poor, 5=excellent). A random sample of 1000 model outputs is automatically scored with GPT-4o, and five attending orthopaedists independently evaluate 200 of them. Agreement between GPT-4o and the human panel yields Cohen’s $\kappa = 0.74$, while inter-expert agreement reaches $\kappa = 0.82$, indicating good consistency of the evaluation protocol.

C. Baseline

To comprehensively evaluate the performance of OrthoInsight, we selected six mainstream baseline models for comparative analysis, including GPT-4 [34], Claude-3 [35], LLaVA1.5-7B [36], VisualGLM-6b [37] [38], Qwen2-VL-7B [39], and MiniGPT-4 [40]. These models represent the cutting-edge technologies in current multimodal and language generation tasks, encompassing different model architectures and optimization strategies, thus providing a multidimensional reference for the comparative analysis.

D. Implementation Details

In our experiments, we conduct all training and inference on a workstation running Ubuntu 20.04, equipped with an Intel(R) Xeon(R) Platinum 8255C CPU (12 vCPUs @ 2.50GHz) and three NVIDIA RTX 3090 GPUs (24 GB). All models are implemented in Python 3.8 with PyTorch 1.11.0 and deployed using CUDA 11.3. The dataset is partitioned into training, validation, and test splits with a ratio of 7:1:2. For the object detection task, we adopt YOLOv9 as the baseline detector. The model is trained with an input image size of 640×640 , a batch size of 16, and 150 training epochs. The initial learning rate is set to 0.01 using cosine annealing. For the report generation task, we use LLaVA-1.5-7B as the base multimodal model and apply parameter-efficient fine-tuning via LoRA. The LoRA configuration includes a rank of 64, an α of 16, and a dropout rate of 0.05. We train for 20 epochs with a batch size of 10 and a learning rate of $1e-4$, requiring approximately 60 hours on three RTX 3090 GPUs.

VII. EXPERIMENTS

To comprehensively validate the effectiveness of the proposed OrthoInsight framework, we design a series of experiments centered around three key evaluation tasks, leading to the following research questions: (1) **RQ1**: Can the YOLOv9 model adopted in OrthoInsight achieve high-precision localization and classification in rib fracture detection? (2) **RQ2**: In diagnostic report generation, does OrthoInsight significantly outperform existing multimodal baselines in terms of content accuracy, completeness, and clinical applicability? (3) **RQ3**: Do the core components of OrthoInsight—such as knowledge graph retrieval, expert report integration, and multi-stage instruction design—contribute substantially to the final report quality?

A. Experimental Validation of YOLOv9 Model(RQ1)

In order to verify the effectiveness of the proposed algorithm, experiments were conducted based on YOLOv9 model, and its performance in the detection of rib fractures was evaluated. YOLOv9 was used as the baseline model for comparison. In the experiments, the algorithm achieved a precision (P) of 98.3%, a recall (R) of 89%, and a mean average precision (mAP) at IoU threshold 0.5 of 74.2%. These results demonstrate that the proposed algorithm performs effectively in substation equipment defect detection, showcasing strong detection capability.

B. Evaluation of Diagnostic Reports RQ2

We redesigned the scoring process by introducing a large language model (LLM)-based automated scoring mechanism to reduce reliance on manual annotations. Specifically, we randomly selected 1,000 samples from the dataset and used OpenAI’s GPT-4 Turbo for automated scoring. To ensure the reliability of the scoring results, Five senior orthopedic experts were invited to manually score 200 samples from these based on predefined evaluation criteria. By combining automated scoring and human evaluation, this study maintained scoring efficiency while enhancing the objectivity and consistency of the evaluation results. To further validate the reliability of the evaluation results, three statistical methods—Kendall’s Tau, Pearson correlation coefficient, and Fleiss’ Kappa—were applied to analyze the consistency of expert ratings, with the results shown in Table III. The analysis indicated a high level of consistency, with Kendall’s Tau coefficients all above 0.7 (accuracy 0.85, clarity 0.88), Pearson correlation coefficients close to 0.9 (accuracy 0.92, overall rating 0.91), and Fleiss’ Kappa values all above 0.7 (clarity 0.80, accuracy 0.76).

TABLE III
CONSISTENCY ANALYSIS OF SCORING RESULTS

Metric	Kendall’s Tau	Pearson	Fleiss’ Kappa
DA	0.85	0.92	0.76
CC	0.88	0.90	0.80
LCC	0.73	0.85	0.70
CGV	0.78	0.87	0.72
Average	0.82	0.91	0.74

These findings further validated the reliability and consistency of the scoring process. In terms of specific scores, OrthoInsight achieved scores of 4.32, 4.11, 4.41, and 4.27 for Diagnostic Accuracy, Content Completeness, Logical Coherence and Consistency, and Clinical Guidance Value, respectively, with an average score of 4.28 (as shown in Table IV). All evaluation metrics scored above 4, demonstrating the model’s exceptional performance in generating high-quality diagnostic reports. In contrast, although GPT-4 and Claude-3 performed well in some metrics, their overall scores were slightly lower, highlighting the advantages of our knowledge enhancement approach and customized model design. Additionally, LLaVA1.5-7B, as the base model for OrthoInsight, achieved the best performance among models of a similar scale, further demonstrating its strength and reliability as a foundational model.

C. Ablation Experiment (RQ3)

To validate the effectiveness of each method, we designed and conducted ablation experiments, testing SFT only, knowledge enhancement only, and replacing knowledge enhancement with Zero-shot-CoT to analyze the contribution of different modules to model performance. As shown in Table V, the SFT method demonstrated the most significant improvement across various performance metrics. By applying SFT, the model was better adapted to specific task scenarios, achieving targeted optimization and exhibiting higher accuracy

TABLE IV
ORIGINAL SCORE SHEET

	Model	DA.	CC.	LCC.	CGV.	Avg.
GPT4 scorer	GPT4	3.51	3.29	3.41	3.27	3.37
	Claude3	3.26	3.17	3.56	3.21	3.30
	LLAVA1.5-7B	3.02	2.97	3.16	2.83	3.05
	VisualGLM-6B	2.83	3.04	2.81	2.83	2.89
	Qwen2-VL-7B	2.79	2.71	3.03	2.79	2.83
	MiniGPT-4	2.28	2.38	2.48	2.51	2.41
	OrthoInsight	4.41	4.16	4.44	4.39	4.35
Expert rating	GPT4	3.43	3.37	3.35	3.25	3.35
	Claude3	3.30	3.46	3.50	3.23	3.38
	LLAVA1.5-7B	2.94	3.01	3.11	2.87	2.98
	VisualGLM-6B	2.83	3.04	2.91	2.83	2.90
	Qwen2-VL-7B	2.79	2.76	3.03	2.86	2.86
	MiniGPT-4	2.33	2.42	2.53	2.46	2.44
	OrthoInsight	4.32	4.11	4.41	4.27	4.28

TABLE V
ABLATION EXPERIMENT SCORE COMPARISON TABLE

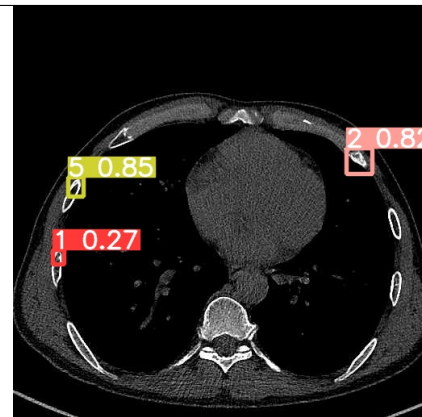
Model	Acc.	Cla.	Com.	Pra.	Ave.
Original	2.94	3.01	3.11	2.87	2.98
SFT	3.62	3.54	3.64	3.53	3.58
COT	3.07	3.09	3.22	3.01	3.10
KE.	3.23	3.27	3.24	3.26	3.25
SFT-COT	3.71	3.62	3.74	3.66	3.68
SFT-KE.	4.41	4.16	4.44	4.39	4.35

and stability in professional tasks. Although the performance of the knowledge enhancement method alone was not as strong as that of SFT, it still played a positive role in supplementing domain knowledge and enhancing task comprehension. When knowledge enhancement was combined with SFT, the model’s overall performance improved further, validating the effectiveness of their synergy. This indicates that the knowledge enhancement method provides the model with enriched background information and professional prompts, helping to generate more accurate and comprehensive responses. In contrast, the performance of the Zero-shot-CoT method was relatively limited, possibly due to the lack of domain-specific prompts, which hindered its task comprehension and detailed response generation. This further demonstrates the importance of professional knowledge prompts in multimodal tasks and complex professional scenarios. Overall, the experimental results show that both SFT and knowledge enhancement play crucial roles in improving model performance, and their combination offers significant advantages in enhancing model adaptability and overall performance.

VIII. CASE STUDY

This section presents a CT imaging diagnostic report generated by OrthoInsight, with high-quality diagnostic content highlighted in green. Table VI provides a detailed case example. In this case, OrthoInsight successfully identified common types of rib fractures and accurately assessed their freshness, alignment status, and risk of complications. Specifically, the system not only differentiates between fresh and old fractures but also provides detailed analyses of fracture stability, local soft tissue response, and potential complications. Compared to traditional reports derived from standard radiology datasets,

TABLE VI
SAMPLED CASE



Diagnostic picture
Diagnostic report

Imaging Findings:

1. Discontinuity of the cortical bone in the anterior segments of the left 4th and 5th ribs, indicating fractures. The alignment of the fracture ends is sub-optimal, with mild displacement. Mild soft-tissue swelling is observed in the surrounding area, while no significant thickening of the adjacent pleura is noted.
2. Linear fracture shadows are observed in the posterior segments of the right 8th and 9th ribs. The fracture ends are well-aligned, and mild bone hyperplasia with callus formation is visible. No abnormal signal is detected in the surrounding soft tissues.
3. No obvious signs of hemothorax or pneumothorax are observed. The mediastinum remains in its normal position, and no distinct consolidation or abnormal opacities are detected in the lung parenchyma.

Imaging Diagnosis:

1. Acute fractures of the anterior segments of the left 4th and 5th ribs, accompanied by mild soft-tissue swelling. No apparent signs of hemothorax or pneumothorax.
2. Old fractures of the posterior segments of the right 8th and 9th ribs, with callus formation and good healing progression.
3. No mediastinal displacement or pulmonary parenchymal lesions detected.

Clinical Recommendations:

1. **Activity restriction:** Limit thoracic movements and avoid vigorous coughing or significant postural changes to reduce the risk of further displacement of the fracture ends.
2. **Pain management:** Non-steroidal anti-inflammatory drugs (NSAIDs) may be used for analgesia. If necessary, elastic chest bandaging can be considered to alleviate chest-wall pain and prevent respiratory distress.
3. **Complication monitoring:** Observe for any signs of delayed pneumothorax or hemothorax, especially if symptoms such as dyspnea, persistent chest pain, or decreased breath sounds develop.
4. **Imaging follow-up:** A follow-up chest CT is recommended in 2–4 weeks to assess fracture healing. If displacement risk persists, further therapeutic interventions may be considered.

OrthoInsight’s diagnostic report demonstrates greater professionalism and specificity. Standard reports typically focus on fracture location and basic imaging descriptions. In contrast, OrthoInsight offers a more comprehensive interpretation, including fracture alignment assessment, imaging characteristics of callus formation, soft tissue response, and a complete evaluation of the mediastinum and lungs. Additionally, this report incorporates explicit clinical management recommendations, covering activity restriction, pain management, complication monitoring, and imaging follow-up, thereby enhancing its practicality and applicability. During the report generation process, OrthoInsight exhibits outstanding imaging analysis capabilities and clinical decision support, aiding radiologists in improving diagnostic efficiency and ensuring that patients

receive more targeted treatment plans. This AI-driven imaging reporting system not only enhances the accuracy and depth of imaging diagnostics but also provides clinicians with high-quality reference information, fostering advancements in intelligent medical imaging.

IX. CONCLUSION

In this study, we present OrthoInsight, a multi-modal deep learning framework for automated rib fracture diagnosis and reporting from CT images. Integrating YOLOv9 for detection, a medical knowledge graph for contextual understanding, and LLaVA for report generation, OrthoInsight addresses limitations of manual interpretation, such as inefficiency and error-proneness. Evaluated on a comprehensive dataset using rigorous metrics, the framework outperforms state-of-the-art models with an average score of 4.28 across diagnostic accuracy, content completeness, logical coherence, and clinical guidance. OrthoInsight not only accurately detects and classifies rib fractures but also generates detailed, clinically meaningful reports, supporting radiologists in decision-making and improving diagnostic efficiency. While promising, the current implementation is research-oriented and not a substitute for professional medical judgment. Future work will focus on expanding dataset diversity, enhancing model robustness, and exploring broader applications in medical imaging.

X. ETHICS STATEMENT

OrthoInsight was developed solely for research purposes and is not intended to provide medical advice or replace professional healthcare expertise. All medical data used, including CT images and expert reports, were obtained from publicly available sources in compliance with ethical standards. While OrthoInsight uses advanced multi-modal models to assist with rib fracture diagnosis and report generation, its outputs may not always be accurate or reliable due to inherent AI limitations. Therefore, the generated reports should not be considered a substitute for professional medical judgment. Individuals with health concerns should consult licensed physicians for proper diagnosis and treatment. This study is committed to scientific transparency, and all methods and results are shared to support further research. Any clinical application of OrthoInsight would require formal regulatory approval beyond the scope of this work.

REFERENCES

[1] B.C. Chapman, D.M. Overbey, and F. Tesfalidet. Clinical utility of chest computed tomography in patients with rib fractures. *Arch Trauma Res*, 5(4):e37070, 2016.

[2] C. Liu, Z. Chen, J. Xu, and G. Wu. Diagnostic value and limitations of ct in detecting rib fractures and analysis of missed rib fractures: a study based on early ct and follow-up ct as the reference standard. *Clinical Radiology*, 77(4):283–290, 2022.

[3] Marta N. Flory, Sandy Napel, and Emily B. Tsai. Artificial intelligence in radiology: Opportunities and challenges. *Seminars in Ultrasound, CT and MRI*, 45(2):152–160, 2024. Perspectives in Radiology Practice: Challenges and Opportunities.

[4] L. Sun, Y. Fan, S. Shi, M. Sun, Y. Ma, K. Zhang, and et al. Ai-assisted radiologists vs. standard double reading for rib fracture detection on ct images: A real-world clinical study. *PLoS ONE*, 20(1):e0316732, 2025.

[5] Y. LeCun, L. Bottou, Y. Bengio, and P. Haffner. Gradient-based learning applied to document recognition. *Proceedings of the IEEE*, 86(11):2278–2324, Nov 1998.

[6] J. Redmon, S. Divvala, R. Girshick, and A. Farhadi. You only look once: Unified, real-time object detection. In *Proceedings of the IEEE Conference on Computer Vision and Pattern Recognition (CVPR)*, pages 779–788, Las Vegas, NV, USA, Jun 2016.

[7] T. Li, M. Liao, Y. Fu, and et al. Intelligent detection and grading diagnosis of fresh rib fractures based on deep learning. *BMC Med Imaging*, 25(1):98, Mar 2025.

[8] Chunyuan Li, Cliff Wong, Sheng Zhang, Naoto Usuyama, Haotian Liu, Jianwei Yang, Tristan Naumann, Hoifung Poon, and Jianfeng Gao. Llava-med: Training a large language-and-vision assistant for biomedicine in one day, 2023.

[9] Xuechen Guo, Wenhao Chai, Shi-Yan Li, and Gaoang Wang. Llava-ultra: Large chinese language and vision assistant for ultrasound, 2024.

[10] Chien-Yao Wang, I-Hau Yeh, and Hong-Yuan Mark Liao. Yolov9: Learning what you want to learn using programmable gradient information, 2024.

[11] Haotian Liu, Chunyuan Li, Qingyang Wu, and Yong Jae Lee. Visual instruction tuning, 2023.

[12] K. Singhal, S. Azizi, T. Tu, and et al. Large language models encode clinical knowledge. *Nature*, 620:172–180, 2023.

[13] Harsha Nori, Nicholas King, Scott Mayer McKinney, Dean Carignan, and Eric Horvitz. Capabilities of gpt-4 on medical challenge problems, 2023.

[14] Xingliang Lou, Wenchao Xia, Kai-Kit Wong, Haitao Zhao, Tony Q. S. Quek, and Hongbo Zhu. Power optimization for integrated active and passive sensing in dfrc systems, 2024.

[15] D. Van Veen, C. Van Uden, L. Blankemeier, and et al. Clinical text summarization: Adapting large language models can outperform human experts. *Res Sq*, Oct 2023. Preprint, rs.3.rs-3483777.

[16] L.C. Adams, D. Truhn, F. Busch, A. Kader, S.M. Niehues, M.R. Makowski, and K.K. Bresslem. Leveraging gpt-4 for post hoc transformation of free-text radiology reports into structured reporting: A multilingual feasibility study. *Radiology*, 307(4):e230725, 2023.

[17] Hassan Shakil, Ahmad Farooq, and Jugal Kalita. Abstractive text summarization: State of the art, challenges, and improvements. *Neurocomputing*, 603:128255, October 2024.

[18] Deng Chen, Weiwei Zhang, and Zuohua Ding. Embedding dynamic graph attention mechanism into clinical knowledge graph for enhanced diagnostic accuracy. *Expert Systems with Applications*, 267:126215, 2025.

[19] Kaiwen Zuo, Yirui Jiang, Fan Mo, and Pietro Lio. Kg4diagnosis: A hierarchical multi-agent llm framework with knowledge graph enhancement for medical diagno-

- sis, 2025.
- [20] S.M. Shamimul Hasan and et al. Knowledge graph-enabled cancer data analytics. *IEEE Journal of Biomedical and Health Informatics*, 24(7):1952–1967, 2020.
- [21] Y. Yang, X. Liu, Q. Jin, and et al. Unmasking and quantifying racial bias of large language models in medical report generation. *Commun Med*, 4:176, 2024.
- [22] Tianyu Han, Lisa C. Adams, Jens-Michalis Papaioannou, Paul Grundmann, Tom Oberhauser, Alexei Figueroa, Alexander Löser, Daniel Truhn, and Keno K. Bresslem. Medalpaca – an open-source collection of medical conversational ai models and training data, 2025.
- [23] Zekai Chen, Arda Pekis, and Kevin Brown. Advancing high resolution vision-language models in biomedicine, 2024.
- [24] Jinlong He, Pengfei Li, Gang Liu, Genrong He, Zhaolin Chen, and Shenjun Zhong. Pefomed: Parameter efficient fine-tuning of multimodal large language models for medical imaging, 2025.
- [25] Zhengyuan Yang, Linjie Li, Kevin Lin, Jianfeng Wang, Chung-Ching Lin, Zicheng Liu, and Lijuan Wang. The dawn of lmms: Preliminary explorations with gpt-4v(ision), 2023.
- [26] Duy M. H. Nguyen, Nghiem T. Diep, Trung Q. Nguyen, Hoang-Bao Le, Tai Nguyen, Tien Nguyen, TrungTin Nguyen, Nhat Ho, Pengtao Xie, Roger Wattenhofer, James Zhou, Daniel Sonntag, and Mathias Niepert. Logra-med: Long context multi-graph alignment for medical vision-language model, 2024.
- [27] Eunsuk Chang and Sumi Sung. Use of snomed ct in large language models: Scoping review. *JMIR Medical Informatics*, 12:e62924, Oct 2024.
- [28] Xintian Yang and et al. Application of large language models in disease diagnosis and treatment. *Chinese Medical Journal*, 138(2):130–142, 2025.
- [29] Paul A Tiffin, Gabrielle M Finn, and John C McLachlan. Evaluating professionalism in medical undergraduates using selected response questions: findings from an item response modelling study. *BMC medical education*, 11:1–9, 2011.
- [30] Hongbo Zhang, Junying Chen, Feng Jiang, Fei Yu, Zhihong Chen, Jianquan Li, Guiming Chen, Xiangbo Wu, Zhiyi Zhang, Qingying Xiao, Xiang Wan, Benyou Wang, and Haizhou Li. Huatuogpt, towards taming language model to be a doctor, 2023.
- [31] Yasin Ghafourian, Allan Hanbury, and Petr Knoth. Readability measures as predictors of understandability and engagement in searching to learn. In *International Conference on Theory and Practice of Digital Libraries*, pages 173–181. Springer, 2023.
- [32] Shiromi Karunaratne and Dilshi Dharmarathna. A review of comprehensiveness, user-friendliness, and contribution for sustainable design of whole building environmental life cycle assessment software tools. *Building and Environment*, 212:108784, 2022.
- [33] GG Landis JRKoch. The measurement of observer agreement for categorical data. *Biometrics*, 33(1):159174, 1977.
- [34] State Grid Corporation of China. 95598 intelligent interactive service (official portal), 2025. Accessed Oct. 31, 2025.
- [35] Anthropic. The claude 3 model family: Opus, sonnet, haiku, 2024.
- [36] Haotian Liu, Chunyuan Li, Yuheng Li, and Yong Jae Lee. Improved baselines with visual instruction tuning, 2024.
- [37] Zhengxiao Du, Yujie Qian, Xiao Liu, Ming Ding, Jiezhong Qiu, Zhilin Yang, and Jie Tang. Glm: General language model pretraining with autoregressive blank infilling. In *Proceedings of the 60th Annual Meeting of the Association for Computational Linguistics (Volume 1: Long Papers)*, pages 320–335, 2022.
- [38] Ming Ding, Zhuoyi Yang, Wenyi Hong, Wendi Zheng, Chang Zhou, Da Yin, Junyang Lin, Xu Zou, Zhou Shao, Hongxia Yang, et al. Cogview: Mastering text-to-image generation via transformers. *Advances in Neural Information Processing Systems*, 34:19822–19835, 2021.
- [39] Peng Wang, Shuai Bai, Sinan Tan, Shijie Wang, Zhihao Fan, Jinze Bai, Keqin Chen, Xuejing Liu, Jialin Wang, Wenbin Ge, Yang Fan, Kai Dang, Mengfei Du, Xuancheng Ren, Rui Men, Dayiheng Liu, Chang Zhou, Jingren Zhou, and Junyang Lin. Qwen2-vl: Enhancing vision-language model’s perception of the world at any resolution, 2024.
- [40] Deyao Zhu, Jun Chen, Xiaoqian Shen, Xiang Li, and Mohamed Elhoseiny. Minigpt-4: Enhancing vision-language understanding with advanced large language models, 2023.